# Improving Group Robustness on Spurious Correlation via Evidential Alignment

Wenqian Ye University of Virginia Charlottesville, VA, USA wenqian@virginia.edu Guangtao Zheng University of Virginia Charlottesville, VA, USA gz5hp@virginia.edu Aidong Zhang University of Virginia Charlottesville, VA, USA aidong@virginia.edu

# **Abstract**

Deep neural networks often learn and rely on spurious correlations, i.e., superficial associations between non-causal features and the targets. For instance, an image classifier may identify camels based on the desert backgrounds. While it can yield high overall accuracy during training, it degrades generalization on more diverse scenarios where such correlations do not hold. This problem poses significant challenges for out-of-distribution robustness and trustworthiness. Existing methods typically mitigate this issue by using external group annotations or auxiliary deterministic models to learn unbiased representations. However, such information is costly to obtain, and deterministic models may fail to capture the full spectrum of biases learned by the models. To address these limitations, we propose Evidential Alignment, a novel framework that leverages uncertainty quantification to understand the behavior of the biased models without requiring group annotations. By quantifying the evidence of model prediction with second-order risk minimization and calibrating the biased models with the proposed evidential calibration technique, Evidential Alignment identifies and suppresses spurious correlations while preserving core features. We theoretically justify the effectiveness of our method as capable of learning the patterns of biased models and debiasing the model without requiring any spurious correlation annotations. Empirical results demonstrate that our method significantly improves group robustness across diverse architectures and data modalities, providing a scalable and principled solution to spurious correlations.

# **CCS** Concepts

 Computing methodologies → Machine learning algorithms; Learning under covariate shift; Supervised learning by classification.

# Keywords

Spurious correlations, group robustness, uncertainty quantification

# ACM Reference Format:

Wenqian Ye, Guangtao Zheng, and Aidong Zhang. 2025. Improving Group Robustness on Spurious Correlation via Evidential Alignment. In *Proceedings of the 31st ACM SIGKDD Conference on Knowledge Discovery and Data Mining V.2 (KDD '25), August 3–7, 2025, Toronto, ON, Canada*. ACM, New York, NY, USA, 12 pages. https://doi.org/10.1145/3711896.3737002



This work is licensed under a Creative Commons Attribution 4.0 International License. KDD '25. Toronto. ON. Canada

© 2025 Copyright held by the owner/author(s). ACM ISBN 979-8-4007-1454-2/2025/08 https://doi.org/10.1145/3711896.3737002

# 1 Introduction

Deep neural networks trained with empirical risk minimization (ERM) [39] often exhibit spurious biases, i.e., the reliance on spurious correlations to make predictions. Spurious correlations are brittle associations between prediction targets and non-essential features (e.g., background, texture, or secondary objects) [3, 5, 31, 36, 46, 50]. These correlations can lead models to achieve high average accuracy but perform poorly on minority groups where the spurious correlations are absent. For example, consider a cow/camel classification task shown in Figure 1, the training set may be biased so that the camel class is spuriously correlated with desert backgrounds. ERM-trained models tend to rely on the spurious attributes-desert backgrounds-to identify the camel class. This may lead to biased predictions and poor generalization on minority groups where camels are on grass backgrounds [5]. The high discrepancy in generalization across groups caused by spurious correlations is especially problematic in high-stakes applications such as medicine [47], algorithmic fairness [16], and criminal justice [4], where biased predictions can have severe consequences.

Therefore, it is crucial to improve a model's group robustness, i.e., ensuring generalization across data groups with varying spurious correlations. Group robustness is typically measured by the model's worst accuracy across groups [31]. In practice, the groups are formulated with group labels that pair samples' class labels with their associated spurious attributes, explicitly indicating the correlations that a model may learn. The group labels can be used to construct balanced groups [18, 51, 52] or minimize the worst-group loss [31] to learn invariant representations. Moreover, studies have demonstrated that retraining classifiers on a group-balanced heldout dataset or on samples representing the failures of a biased model can significantly enhance group robustness [17, 25, 28, 45, 53]. However, obtaining group labels can be prohibitively expensive in many real-world applications and these labels sometimes cannot accurately reflect the subtle biases learned by a model. To address these challenges, recent research has focused on group label estimation with biased auxiliary models or sample reweighting mechanisms as alternative strategies for improving a model's group robustness.

Despite significant progress in improving group robustness, existing methods typically rely on external group annotations, which are both costly and labor-intensive to obtain. In addition, most existing annotation-free approaches use deterministic procedures to identify and mitigate spurious biases. This offers only a narrow perspective on how models exploit spurious correlations. Consequently, these methods may not capture the full range of biases present in real-world data. These limitations underscore the need for scalable, annotation-free approaches that provide a more comprehensive understanding of spurious biases.

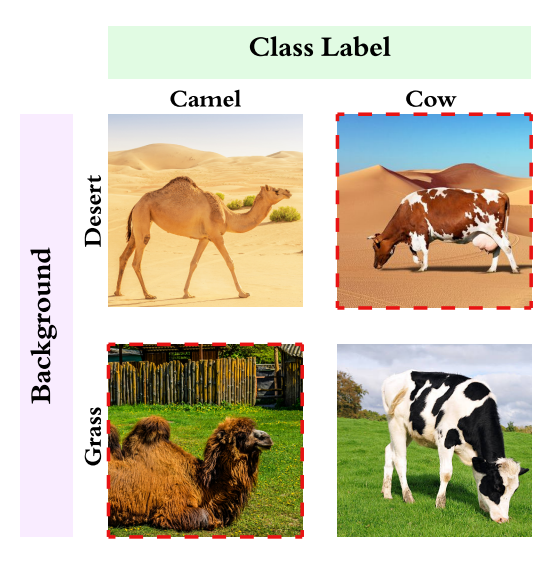


Figure 1: An example of cow/camel classification task. Red dotted lines denote the minority groups where spurious correlation does not hold.

To overcome the limitations of current group robustness techniques, we propose a novel framework equipped with uncertainty estimation to gain deeper insights into spurious biases. Uncertainty can be commonly divided into aleatoric (data) and epistemic (model) uncertainty. In particular, we focus on the epistemic (model) uncertainty as it provides critical information about a model's confidence when it encounters ambiguous data [12, 14]. Such information provides insights into the data in minority groups, which is challenging for a model with spurious biases and is the bottleneck in the model's group robustness. We leverage the Dempster-Shafer Theory of Evidence (DST) [43] to provide a general and well-defined theoretical framework for reasoning with uncertainty. Recent advances in uncertainty quantification [1, 33] have introduced scalable methods for estimating model uncertainty in a single-pass nature without requiring explicit priors such as group annotations. Building on these insights, we propose Evidential Alignment, a novel framework that enhances group robustness without group annotations.

Our approach first augments traditional logit-based prediction probabilities with an uncertainty measure by transforming the objective of a biased ERM model from first-order risk minimization to second-order risk minimization, which refers to learning a distribution over distributions. By modeling uncertainty with a Dirichlet distribution, the model produces both prediction probabilities and an uncertainty estimate. We then apply an evidential calibration procedure to suppress spurious biases while preserving core features via an automatic reweighting process with a calibration dataset. Unlike traditional approaches that depend on external annotations or deterministic bias estimation, Evidential Alignment leverages model uncertainty to automatically detect and mitigate spurious correlations. This uncertainty-guided strategy provides a data-driven measure to pinpoint where the model excessively relies on non-causal features, enabling dynamic adaptation without requiring additional group labels. As a result, our method integrates

seamlessly into standard ERM training, offering a scalable, effective solution for improving group robustness and overall model generalization.

The main **contributions** of this paper are as follows:

- We propose Evidential Alignment, a novel framework that integrates second-order risk minimization and evidential calibration to leverage model uncertainty for identifying and mitigating spurious correlations without group annotations.
- We provide theoretical insights into how uncertainty quantification can capture spurious biases in latent space, offering a principled explanation for the improved robustness of our approach.
- Extensive experiments across diverse architectures and data modalities demonstrate that Evidential Alignment significantly enhances group robustness and generalization <sup>1</sup>.

# 2 Related Works

**Spurious Correlations.** The limitations of empirical risk minimization (ERM) in the presence of spurious correlations have been widely studied. In vision modality, ERM-trained models frequently rely on non-causal features such as background, texture, and secondary objects for classification. Similarly, in language modality, these models often exploit syntactic or statistical heuristics instead of true semantic understanding. Such reliance on spurious correlations can result in biased predictions against demographic minorities and lead to failures in high-stakes applications.

Group Robustness Methods. Existing approaches to improve group robustness against spurious correlations can be categorized based on their reliance on external supervision. Supervised methods require explicit group annotations that identify spurious correlations in the training data. If group annotations are available in the training dataset, group distributionally robust optimization (Group DRO) [31] can improve group robustness by minimizing the worstcase loss across predefined groups, while other methods[2, 10, 48] learn invariant and diverse features via different techniques. Methods that only use partial group annotations include deep feature reweighting (DFR) [18], which retrains the final layer of the model on a group-balanced held-out set, and spread spurious attribute [29], which only optimizes Group DRO with pseudo group labels. Moreover, several methods [40] focus on lightweight post-hoc approaches to debias the models. Since the groups are often unknown and require expert knowledge to annotate in real-world applications, there has been great interest in methods which do not explicitly require group annotation except for model selection. Several methods[17, 25, 28] utilize auxiliary models to pseudo-label the minority group or spurious attribute. A recent work [24] proposed an unsupervised approach that upweights misclassified samples from a bias-amplified model and selects models based on minimum class difference. While promising, this method still relies on deterministic auxiliaries for bias amplification, which may not fully capture the spurious biases. In contrast, our approach leverages uncertainty-aware information from biased models in a fully unsupervised manner. By quantifying model uncertainty and calibrating the biased model, we provide a broader perspective on identifying

 $<sup>^1\</sup>mathrm{Our}$  code is available at https://github.com/wenqian-ye/evidential\_alignment

and mitigating spurious correlations without requiring any group annotations.

Uncertainty Quantification. Uncertainty quantification is crucial for assessing the reliability of deep learning models, particularly in safety-critical applications. Uncertainty is typically divided into aleatoric uncertainty (from inherent data noise) and epistemic uncertainty (from limited knowledge about model parameters) [14]. Methods like Bayesian Neural Networks [7], Monte Carlo Dropout [9], and Deep Ensembles [22] estimate uncertainty with multiple model parameters or multiple passes, which can be computationally intensive. These uncertainty quantification methods [9, 22] involve higher computational overhead and multiple model passes, thus not in our scope. Evidential deep learning [33] offers an efficient yet effective alternative by modeling evidence as parameters of a Dirichlet distribution, capturing both uncertainties without the need for sampling or ensembles. While uncertainty quantification has been applied to model calibration, active learning, and out-ofdistribution detection, its use in improving group robustness is less explored. Building on these insights, our method employs epistemic uncertainty to adaptively reweight samples during retraining, reducing the model's reliance on spurious attributes without requiring explicit group labels.

# **Problem Formulation**

### **Preliminaries**

We consider a classification problem with a training set  $\mathcal{D}_{train}$  =  $\{(x,y)|x\in\mathcal{X},y\in\mathcal{Y}\}$ , where x is a sample in the input space X and y is the corresponding label in the finite label space  $\mathcal{Y}$ . The training data is composed of groups  $\mathcal{D}_g^{\mathrm{tr}}$ , such that  $\mathcal{D}_{\mathrm{train}} = \cup_{g \in \mathcal{G}} \mathcal{D}_g^{\mathrm{tr}}$ . Each group g := (y, a) is defined by a class label  $y \in \mathcal{Y}$  and a spurious attribute  $a \in \mathcal{A}$ , where  $\mathcal{A}$  is the set of all spurious attributes in  $\mathcal{D}_{\text{train}}$ , and  $\mathcal{G}$  is the set of all possible group labels. A group  $\mathcal{D}_{a}^{\text{tr}}$ consists of sample-label pairs (x, y) sharing the same y and a.

Our goal is to learn a model  $f_{\theta}: \mathcal{X} \to \mathcal{Y}$ , parameterized by  $\theta$ from the parameter space  $\Theta$ , that generalizes well across all groups on the test set  $\mathcal{D}_{test}$ . The standard approach is Empirical Risk Minimization (ERM), which minimizes the expected training loss:

$$\mathcal{L}_{\text{ERM}}(f_{\theta}; x, y) = \min_{\theta \in \Theta} \mathbb{E}_{(x, y) \sim \mathcal{D}_{\text{train}}} \left[ \ell(f_{\theta}(x), y) \right], \tag{1}$$

where  $\ell$  is a loss function. However, ERM-trained models often exploit spurious attributes and underperform on minority groups. To address this, we frame the group robustness problem as a minmax optimization:

$$\min_{\theta \in \Theta} \max_{g \in \mathcal{G}} \mathbb{E}_{(x,y) \sim \mathcal{D}_g^{\text{tr}}} \left[ \ell(f_{\theta}(x), y) \right], \tag{2}$$

where  $\mathcal{D}_{q}^{\text{tr}}$  is the training data from group g. This ensures the model performs well even on minority groups.

# **Uncertainty Decomposition**

In probabilistic modeling, uncertainty is commonly divided into aleatoric (data) and epistemic (model) uncertainty. These two notions can be revealed when formulating the posterior predictive distribution of a classifier  $\theta$  for a new data point  $(x, y) \in \mathcal{D}$ . In the following, we decompose the expression to show the foundation of our methodological design. First, we decompose uncertainty into

aleatoric (data) and epistemic (model) uncertainty by marginalizing on  $\theta$ , i.e.,

$$p(y|x) = \int \underbrace{P(y|x,\theta)}_{\text{Aleatoric}} \underbrace{p(\theta|\mathcal{D})}_{\text{Epistemic}} d\theta. \tag{3}$$

For a large number of real-valued parameters  $\theta$  like in neural networks, this integral becomes intractable to evaluate, and thus is usually approximated using Monte Carlo samples which could incur significant computational overhead and approximation errors. To address this, a line of works [12, 27, 37] propose to factorize Equation (3) further:

$$p(y|x) = \iint \underbrace{P(y|\boldsymbol{\pi})}_{\text{Aleatoric Distributional Epistemic}} \underbrace{p(\theta|\mathcal{D})}_{\text{Epistemic}} d\boldsymbol{\pi} d\theta \qquad (4)$$

$$= \int P(y|\boldsymbol{\pi}) \underbrace{p(\boldsymbol{\pi}|x,\hat{\theta})}_{p(\theta|\mathcal{D}) = \delta(\theta - \hat{\theta})} d\boldsymbol{\pi}. \qquad (5)$$

$$= \int P(y|\boldsymbol{\pi}) \underbrace{p(\boldsymbol{\pi}|x,\hat{\theta})}_{p(\theta|\mathcal{D}) = \delta(\theta - \hat{\theta})} d\boldsymbol{\pi}. \tag{5}$$

In Equation (3), we use a probabilistic distribution  $\pi$  to capture the distributional behavior of the data. Also, we can replace  $p(\theta|\mathcal{D})$ with a point estimate  $\hat{\theta}$  using the Dirac delta function, i.e., a single trained neural network, to get rid of the intractable integral. Although another integral remains, retrieving the uncertainty from this predictive distribution has a closed-form analytical solution for the Dirichlet distribution.

# Methodology

We propose Evidential Alignment, a two-stage approach to improve group robustness without group labels shown in Figure 2. In the first stage, we extend standard ERM to a second-order risk minimization paradigm, enabling the model to estimate both predictions and their corresponding epistemic uncertainty. In the second stage, we apply an evidential calibration approach with a calibration dataset, i.e., using overconfident samples to systematically correct the model's biases. Below, we formalize each component.

### Second-order Risk Minimization

Let  $(x, y) \in \mathcal{D}_{train}$  denote a training sample. Conventional firstorder methods such as ERM optimize a deterministic predictive distribution  $p(y|\theta,x)$  by directly estimating parameters  $\theta$  (e.g., classification logits), which minimize empirical risk via objectives like negative log-likelihood. While effective for average performance, these methods conflate aleatoric (data) uncertainty and epistemic (model) uncertainty, and often exhibit brittleness under distribution shifts or spurious correlations.

Second-order risk minimization addresses this limitation by modeling a distribution over distributions  $p(\theta|\pi(x))$ , where  $\pi(x)$ parameterizes uncertainty about the prediction outcomes. Inspired by previous works [33, 37], we extend the ERM model  $f_{\theta}$  to output evidence values. Let the biased model parameter  $\theta = (\phi_{\theta}, h_{\theta})$  decompose into a feature extractor  $\phi_{\theta}$  and classifier  $h_{\theta}$ . Our goal is to learn the parameters  $\theta_1 = (\phi_{\theta_1}, h_{\theta_1})$  and a distribution which can jointly represent both classification objective and uncertainty quantification. As proved in [6], Dirichlet distribution allows us to use

#### (a) Second-order Risk Minimization (b) Evidential Calibration $f_{\theta_2}$ Dirichlet Distribution $f_{\theta_1}$ Feature Classifier Extractor Calibration Data Feature Classifier $\mathcal{D}_{ ext{calib}}$ Extractor Ontimize $e_K$ Training Data Reweighted Class Balancing $\mathcal{D}_{ ext{train}}$ Latent Classes Loss Embeddings $k = 1, 2, \cdots, K$ Uncertainty $i = 1, 2, \dots, N$ и

Figure 2: Overall framework of Evidential Alignment. (a) Extract the latent embeddings and train the classifier along with the Dirichlet distribution parameters using second-order risk minimization. (b) Compute the uncertainty for the calibration dataset  $\mathcal{D}_{\text{calib}}$  and apply a reweighted loss with class-balanced sampling to refine the classifier.

the principles of evidential theory to quantify belief masses and uncertainty through a well-defined theoretical framework. The parameters of the Dirichlet distribution  $\alpha(x) = [\alpha_1(x), \alpha_2(x), \dots, \alpha_K(x)]$  over K classes are defined as:

$$\alpha_k(x) = e_k(x) + 1, \quad \text{for } k = 1, \dots, K,$$
 (6)

where  $e_k \ge 0$  (k = 1,...,K) is the evidence derived for the k-th singleton. The non-negative evidence  $e_k(x)$  for each class  $k \in \{1,...,K\}$  is derived from the model outputs from classifier  $h_{\theta_1}$ . The Dirichlet distribution over the class probabilities, that is,  $\mathbf{p}(x) = [p_1(x), p_2(x),...,p_K(x)]$ , can be expressed as:

$$\operatorname{Dir}(\mathbf{p}(x) \mid \boldsymbol{\alpha}(x)) = \frac{1}{B(\boldsymbol{\alpha}(x))} \prod_{k=1}^{K} p_k(x)^{\alpha_k(x) - 1}, \tag{7}$$

where  $B(\boldsymbol{\alpha}(x))$  is the multivariate Beta function. The expected class probabilities are:

$$\mathbb{E}[p_k(x)] = \frac{\alpha_k(x)}{S(x)}, \quad \text{where } S(x) = \sum_{k=1}^K \alpha_k(x). \tag{8}$$

By analyzing both the prediction results and the corresponding uncertainty estimates, we can gain valuable insights on how the model is influenced by the training data distribution. For a classification task with K classes, the model outputs non-negative evidence values  $e_k(x) \geq 0$  for each class k.

To guide the learning of both prediction and the parametrization of Dirichlet distribution, we formulate the loss function for **second-order risk minimization** as:

$$\mathcal{L}_{1}(x,y|\theta_{1}) = \underbrace{-\log(\mathbb{E}[p_{y}(x)])}_{\text{Classification Objective}} + \lambda \cdot \underbrace{\text{KL}(\text{Dir}(\boldsymbol{\alpha}(x)) \parallel \text{Dir}(\mathbf{1}))}_{\text{Evidence Regularization}},$$
(9)

where  $\lambda$  is an evidence regularization coefficient and Dir(1) represents a non-informative Dirichlet prior with all concentration parameters equal to 1. The Evidence Regularization term penalizes

overconfidence and promotes uncertainty where appropriate. We first define the classification objective as follows.

$$\mathcal{L}_{\text{cls}}(x, y | \theta_1) = -\log(\frac{\alpha_y(x)}{S(x)}) = -\log(\frac{e_y(x) + 1}{\sum_{k=1}^{K} (e_k(x) + 1)}). \quad (10)$$

For the Evidence Regularization term, it controls overconfidence by penalizing large deviations from the uniform prior. It is defined as the Kullback-Leibler (KL) divergence between the predicted Dirichlet distribution and a non-informative prior (a uniform Dirichlet distribution).

$$KL(Dir(\boldsymbol{\alpha}) \parallel Dir(\mathbf{1})) = \log(\frac{B(\mathbf{1})}{B(\boldsymbol{\alpha})}) + \sum_{k=1}^{K} (\alpha_k - 1)(\psi(\alpha_k) - \psi(S)),$$
(11)

where  $\psi(\cdot)=\frac{d}{dz}\ln\Gamma(\cdot)$  is the digamma function. The loss for a sample  $(x,y)\in\mathcal{D}_{\mathrm{train}}$  becomes:

$$\mathcal{L}_{1}(x,y|\theta_{1}) = -\log\left(\frac{e_{y}(x) + 1}{\sum_{k=1}^{K} (e_{k}(x) + 1)}\right) + \lambda_{t} \cdot \text{KL}(\text{Dir}(\boldsymbol{\alpha}(x)) \parallel \text{Dir}(\mathbf{1})). \tag{12}$$

In practice, we adopt a dynamic evidence regularization coefficient  $\lambda_t = \min(\frac{t}{\eta}, 1)$  to stabilize the training process, where t is the current epoch number and  $\eta$  is a hyperparameter of the annealing step.

# 4.2 Evidential Calibration

After training the model with the second-order risk, we use the estimated epistemic uncertainty to compute a weight for each sample (x,y) in the calibration set  $\mathcal{D}_{\text{calib}}$ , then calibrate the biased model. As shown in Equation (5), the predictive distribution can be expressed via  $p(y|\pi)$  and  $p(\pi|x,\hat{\theta})$ . In this stage, we aim to

learn unbiased representation based on the estimated epistemic uncertainty.

Firstly, we can compute the uncertainty estimate u(x) from the learned Dirichlet distribution.

$$u(x) = \frac{K}{S(x)} = \frac{K}{\sum_{k=1}^{K} \alpha_k(x)},$$
(13)

where S(x) is the sum of the Dirichlet parameters from the learned evidential model. Higher values of u(x) suggest larger epistemic uncertainty in the prediction for sample x. To perform Bayesian model averaging (BMA) during retraining, we integrate the estimated posterior probabilities by reweighting the loss contributions with class-balanced samples.

We express the reweight function w(x,y) in the calibration dataset  $\mathcal{D}_{\mathrm{calib}}$ :

$$w(x,y) = \mathbb{1} \left[ f_{\theta_{1}}(x) = y \right] + u(x) \cdot \mathbb{1} \left[ f_{\theta_{1}}(x) \neq y \right], \tag{14}$$

where  $\mathbb{1}[\cdot]$  is the indicator function. This upweights misclassified samples proportionally to their epistemic uncertainty. The objective function for retraining the model parameters  $\theta_2$  over the calibration dataset  $\mathcal{D}_{\text{calib}}$  becomes:

$$\mathcal{L}_{2}(\mathcal{D}_{\text{calib}}|u,\theta_{2}) = \underset{(x,y) \sim \mathcal{D}_{\text{calib}}}{\mathbb{E}} \left[ w(x,y) \, \ell_{\text{ce}} \left( f_{\theta_{2}}(x), y \right) \right] + \beta \left\| \theta_{2} - \theta_{1} \right\|_{2}^{2}, \tag{15}$$

where  $\ell_{\rm ce}(f_{\theta}(x),y)$  is the cross-entropy loss function for sample (x,y). Here,  $\theta_1$  denotes the parameters learned at the end of second-order risk minimization, and  $\beta$  controls how strongly we regularize the retraining objective. During training, we draw samples from  $\mathcal{D}_{\rm calib}$  in a class-balanced manner.

In practice, we only retrain the last layer of the model to learn the invariant features like previous works [18, 21]. This approach enhances the model's robustness to spurious correlations and improves generalization across all groups without requiring explicit group labels.

# 4.3 Overview of Evidential Alignment

We summarize Evidential Alignment in Algorithm 1. It consists of two stages. The first stage performs second-order risk minimization, where the model estimates uncertainty using a Dirichlet distribution and incorporates a KL regularization. The second stage uses the estimated uncertainty to compute sample weights on a calibration set and retrains the last layer with reweighted loss.

# 4.4 Theoretical Analysis

In this section, we provide theoretical guarantees for our method, demonstrating that (1) second-order risk minimization converges to a Dirichlet distribution of the ERM model, and (2) the PAC-Bayes generalization bound for the reweighted empirical risk holds.

Theorem 4.1 (Evidence Lower Bound for Second-Order Risk). Let  $p(\pi|y)$  be the true posterior distribution over class probabilities given label y, and let  $p(\pi|x,\theta)$  be the variational evidential distribution approximating it, where  $\theta$  represents the model parameters. Then, training with the second-order risk minimization optimizes the evidence lower bound (ELBO), which maximizes the log marginal likelihood of observed labels and learns evidence on the predictions.

### Algorithm 1 Evidential Alignment

```
ased model f_{\theta}, number of epochs T_1, T_2, KL regularization term
 2: Output: Updated model parameters \theta^*
   Stage 1: Second-order Risk Minimization
 4: for epoch t = 1 to T_1 do
        for each sample (x, y) \in \mathcal{D}_{train} do
5:
             Estimate evidence e_k(x) for each class k
7:
             Calculate Dirichlet parameters: \alpha_k(x) = e_k(x) + 1
             Calculate expected class probabilities: \mathbb{E}[p_k(x)]
8:
 9.
             Calculate classification loss: \mathcal{L}_{cls}(x, y|\theta_1)
             Calculate KL Divergence: KL(Dir(\alpha(x)) || Dir(1))
10:
             Optimize last-layer parameters \theta_1 with \mathcal{L}_1(x, y|\theta_1)
11:
        end for
12:
   end for
13:
   Stage 2: Evidential Calibration
    for epoch t = 1 to T_2 do
        for each sample (x, y) \in \mathcal{D}_{calib} do
16:
             Calculate uncertainty: u(x) = \frac{K}{S(x)}
17
             Calculate weights: w(x, y)
18:
             Calculate reweight loss: w(x, y) \cdot \ell(f_{\theta}(x), y)
19:
             Optimize last-layer parameters \theta_2 with \mathcal{L}_2(\mathcal{D}_{\text{calib}}|u,\theta_2)
20:
    end for
```

1: **Input:** Training dataset  $\mathcal{D}_{ ext{train}}$ , calibration dataset  $\mathcal{D}_{ ext{calib}}$ , bi-

Formally, the loss function:

23: **Return:** Updated model parameters  $\theta^*$ 

$$\mathcal{L}_{\text{ELBO}} = \mathbb{E}_{p(\boldsymbol{\pi}|\boldsymbol{x},\boldsymbol{\theta})}[-\log P(\boldsymbol{y}|\boldsymbol{\pi})] + \text{KL}[p(\boldsymbol{\pi}|\boldsymbol{x},\boldsymbol{\theta}) \parallel p(\boldsymbol{\pi})] \quad (16)$$

is an upper bound on the negative log-marginal likelihood –  $\log p(y)$ .

This result informs the core principle of second-order risk minimization: by modeling a Dirichlet distribution for each sample, we impose a Bayesian perspective that naturally captures model confidence and uncertainty.

Theorem 4.2 (PAC-Bayes Bound for Reweighted Empirical Risk). Let  $\mathcal{H}$  be a hypothesis space with [0,1]-bounded loss, and let  $\mathcal{G}=\{1,\ldots,|\mathcal{G}|\}$  be a finite set of latent groups. Suppose we have  $n_g$  i.i.d. training samples from group  $g\in\mathcal{G}$ , and define  $n_{\min}=\min_g n_g$ . Let  $R_g(f)$  be the true risk of hypothesis  $f\in\mathcal{H}$  on group g, and let  $\hat{R}_g(f)$  be the empirical risk of f on the  $n_g$  training samples in group g. Suppose a (potentially data-dependent) weighting scheme  $\{w_g\}_{g\in\mathcal{G}}$  is chosen such that  $w_g\geq 0$  and  $\sum_{g=1}^{|\mathcal{G}|} w_g=1$ . Define the reweighted empirical risk

$$\hat{R}_{w}(f) = \sum_{g=1}^{|\mathcal{G}|} w_{g} \, \hat{R}_{g}(f),$$
 (17)

and let  $\alpha = \min_g w_g$ . Let P be a prior distribution over  $\mathcal{H}$ , and let Q be a (posterior) distribution over  $\mathcal{H}$ . Then, for any  $0 < \delta < 1$ , with probability at least  $1 - \delta$  over the random draw of all training samples,

the worst-group risk of Q satisfies:

$$\max_{1 \le g \le |\mathcal{G}|} \mathbb{E}_{f \sim Q} \left[ R_g(f) \right] \le \frac{1}{\alpha} \mathbb{E}_{f \sim Q} \left[ \hat{R}_w(f) \right] + \sqrt{\frac{\text{KL}(Q \parallel P) + \ln\left(\frac{|\mathcal{G}|}{\delta}\right)}{2 \, n_{\min}}}.$$
(18)

This theorem shows that if a reweighting scheme keeps the reweighted empirical risk low, the worst-group risk remains bounded with high probability. Consequently, optimizing the reweighted empirical risk with a suitably chosen weighting scheme that accounts for the worst-case group leads to better group robustness.

We defer the detailed proofs of both Theorem 4.1 and Theorem 4.2 to the Appendix.

# 5 Experiments

We evaluate Evidential Alignment on a range of group robustness benchmarks and provide ablation studies and additional results to further support our motivation and methodology designs.

#### 5.1 Datasets

We evaluate six benchmark datasets for group robustness in vision and language tasks. We also move beyond simple binary classification tasks that have been the focus of most recent works for studying spurious correlations. Below, we show the dataset details. **Colored MNIST** [2] is a variant of the MNIST dataset designed for image classification, where digit colors introduce spurious correlations with class labels. In our setup, we choose two classes: digit 1 as class 0 and digit 8 as class 1 with two colors green and red as spurious attributes, following Arjovsky et al. [2].

Waterbirds [31] is an image classification dataset with waterbird and landbird classes selected from the CUB dataset [41]. The spurious attribute is the water or land backgrounds from the Places dataset [54], where more landbirds are present on land backgrounds than waterbirds, and vice versa.

**CelebA** [26] is a large scale image dataset with celebrity faces. The task is to identify whether the celebrity's hair color (blonde or non-blonde). The spurious attribute is gender (male and feamale) where the majority group is blonde women in the training set.

**CheXpert** [13] is a large scale clinical dataset of chest radiograph. The dataset includes six spurious attributes, defined by the combination of race (White, Black, Other) and gender (Male, Female). The classification task involves predicting two diagnostic outcomes: "No Finding" (positive) or "Finding" (negative).

**MultiNLI** [42] is a large-scale natural language inference dataset that contains sentence pairs across multiple genres, annotated with entailment classes (entailment, contradiction, and neutral). The spurious attribute involves syntactic or lexical patterns (e.g., negation words) that correlate with specific labels.

**CivilComments** [8] is a binary text classification dataset sourced from internet comments. The task is to predict whether a comment contains toxic language. The spurious attributes include eight demographic identities (e.g., gender, race, etc) that correlate with the label. The dataset uses standard splits from the WILDS benchmark [19].

# 5.2 Experimental Setups

**Training Details.** We first train the ERM base models with pretrained weights. For the image datasets, we use a ResNet-50 [11]

Table 1: Comparison of Test Accuracy on CMNIST between ERM and Ours (%). (Class 1, Color 0) is the minority group.

Accuracy	ERM	Ours
Average	76.34	96.21
Class 0, Color 0	100.00	100.00
Class 0, Color 1	82.81	97.83
Class 1, Color 0	3.74	84.58
Class 1, Color 1	100.00	99.45
WGA	3.74	84.58

model pretrained on ImageNet as the backbone. For the text datasets, we use the BERT-base-uncased model [15] pretrained on the Book-Corpus and English Wikipedia. Consistent with the approach in [44], we don't apply any data augmentations during ERM training. For our method, we constructed the calibration dataset  $\mathcal{D}_{\text{calib}}$  using the same half of the validation set and used it for both second-order minimization and evidential calibration. The remaining half of the validation set is only used for model selection and hyperparameter tuning. During both second-order risk minimization and evidential calibration, we only train the last-layers of the models. We ran the training under three different random seeds and reported average accuracies along with standard deviations. All experiments were conducted on NVIDIA A6000 GPUs. We provide full experimental details in the Appendix.

Model Selection Strategy. We tested three model selection strategies in this work. Using the second half of the validation set, we compute (1) standard average accuracy, which represents the overall classification accuracy across all validation samples, (2) worst-class accuracy, which measures the accuracy on the least accurate class to assess class-wise performance disparities, and (3) worst-group accuracy (WGA), which evaluates the model's performance on the most challenging group, providing insight into its robustness against spurious correlations. In practice, we use worst-class accuracy to make fair comparisons where there are no group labels available. **Evaluation Metric.** We use the worst-group accuracy (WGA) as the main metric for evaluating group robustness, shown in Equation (19). WGA computes the accuracy of test samples that contain the spurious attribute associated with the other class during training. It measures the model's accuracy on the group with the lowest performance.

$$WGA(f_{\theta}; x, y) := \min_{g \in \mathcal{G}} \mathbb{E}_{(x, y) \sim \mathcal{D}_g} [\mathbb{1}[f_{\theta}(x) = y]], \qquad (19)$$

where  $\mathbbm{1}[f_{\theta}(x) \neq y]$  is the 0-1 loss. In addition, we also measure the accuracy gap between standard average accuracy and worst-group accuracy as a measure of the robustness of the models. A high worst-group accuracy and a low accuracy gap indicate that the classifier is robust to spurious correlations and can fairly predict samples from different groups.

# 5.3 Synthetic Experiment

To demonstrate the concept of Evidential Alignment, we first conducted a simple synthetic experiment with the Colored MNIST dataset [2]. In this experiment, we manually introduced spurious

Method Backbone		<b>Group Annotations</b>		Waterbirds			CelebA		
Method Backbone	Train	Val	WGA(%)↑	Acc.(%) ↑	Gap (%) ↓	WGA(%)↑	Acc.(%) ↑	Gap(%) ↓	
ERM [39]	ResNet50	-	-	72.6	97.3	24.7	47.2	95.6	48.4
JTT [25]	ResNet50	No	Yes	86.7	93.3	6.6	81.1	88.0	6.9
CnC [49]	ResNet50	No	Yes	$88.5_{\pm0.3}$	$90.9_{\pm 0.1}$	2.4	$88.8_{\pm 0.9}$	$89.9_{\pm 0.5}$	1.1
AFR [30]	ResNet50	No	Yes	$90.4_{\pm 1.1}$	$94.2_{\pm 1.2}$	3.8	$82.0_{\pm 0.5}$	$91.3_{\pm 0.3}$	9.3
$\mathrm{DFR}^{\dagger}$ [18]	ResNet50	No	Yes	$92.9_{\pm 0.9}$	$94.2_{\pm 0.3}$	2.5	$88.3_{\pm 1.1}$	$91.3_{\pm 0.5}$	3.0
$SELF^{\dagger}$ [21]	ResNet50	No	Yes	$93.0_{\pm 0.3}$	$94.0_{\pm 1.7}$	1.0	$83.9_{\pm 0.9}$	$91.7_{\pm0.4}$	7.8
LfF [28]	ResNet50	No	No	78.0	91.2	13.2	77.2	85.1	7.9
BPA [34]	ResNet50	No	No	71.4	-	-	82.5	-	-

76.2

 $89.1_{\pm 0.2}$ 

92.2 + 0.7

95.7

 $91.4_{\pm 0.3}$ 

95.1+0.5

19.5

2.3

2.9

No

No

No

Table 2: Comparison of worst-group accuracy (WGA), average accuracy (Acc.), and accuracy gap across image datasets. Best worst-group accuracies are highlighted in boldface. † denotes using a fraction of validation data for model fine-tuning.

correlations between the color and the class label, with 90% of the training samples ( $p_{\rm corr}=0.9$ ) exhibiting this color-class association, while only 10% of the test samples ( $p_{\rm corr}=0.1$ ) retained the same correlation. For Class 0, there are 6,398 red instances and 344 green instances. For Class 1, there are 325 red instances and 5,526 green instances. Notably, the (0, green) and (1, red) represent the minority groups in this synthetic dataset.

ResNet50

ResNet50

ResNet50

No

No

No

We used Evidential Alignment to learn group robustness models. First, we trained a simple CNN model, LeNet-5 [23] using ERM with second-order risk minimization for 10 epochs. After obtaining the uncertainty estimates from the ERM model, we calculated the weights and optimize the evidential calibration objective to mitigate the impact of the spurious correlations.

We first show that second-order risk minimization can give a good estimate of challenging samples (in minority groups) in Figure 3 with t-SNE visualization [38]. As shown in Table 1, this approach significantly improves the performance for the minority group (Class 1, Color 0), with accuracy increasing from 3.74% to 84.58%. The performance of the majority groups remains unaffected by the retraining process. Here, the purpose of selecting digits 1 and 8 in this experiment was only to provide a clear contrast between the two classes. Other digit pairs, such as 0 and 7, would yield similar results.

#### 5.4 Main Results

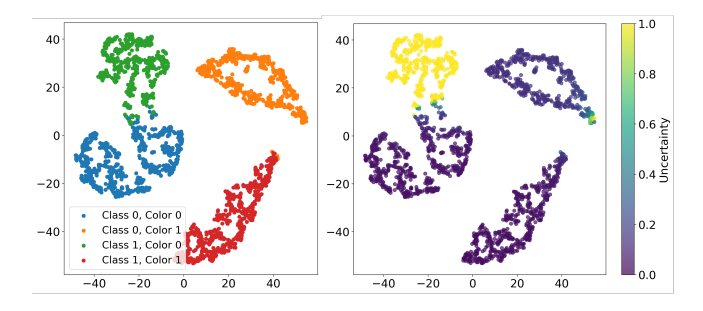
GEORGE [35]

BAM [24]

Ours<sup>†</sup>

In this section, we compare our method, Evidential Alignment, with state-of-the-art baseline methods for improving group robustness, and in particular, with those not requiring group annotations in both training and validation sets. We tested our method on real-world datasets, covering both image and text modalities. We are especially interested in methods that can achieve a high worst-group accuracy (WGA) as well as a low accuracy gap, as such methods demonstrate high group robustness and do not exhibit strong prediction biases towards certain data groups.

As shown in the bottom parts of Tables 2 and 3, which include methods that do not use group annotations, our method achieves the best WGA, demonstrating its superior capability in improving a



52.4

 $80.1_{\pm 3.3}$ 

84.4 + 0.8

94.8

88.4 + 2.3

92.3 + 0.6

42.4

8.3

7.9

Figure 3: t-SNE visualization of the embeddings on the test set with ERM model. Left: test data samples in four groups. Right: quantified uncertainty for each sample (Yellow denotes high uncertainty; Dark purple denotes low uncertainty).

model's group robustness without explicit supervision with group labels. For methods that require group labels for model selection, such as JTT [25] and AFR [30], our method consistently outperforms them in terms of WGA and accuracy gap. We note that CnC [49] achieves the best WGA on CelebA; however, unlike our method, it fails to achieve superior performance on the other datasets. Similar to our method, SELF [21] uses a half of the validation data for training without group labels. Our method outperforms SELF on three out four datasets. DFR [18], which uses group labels in a half of validation data for training, is expected to achieve high WGAs on these datasets. We show that, even without group labels, our method is competitive with DFR and outperforms it on the MultiNLI dataset. In Table 4, we used the CheXpert dataset, which contains chest radiograph confounded with gender and race, as an example to further demonstrate the effectiveness of our method on critical domains. Our method achieves both the best WGA and average accuracy on this dataset, exhibiting strong robustness against spurious attributes.

Notably, our method introduces minimal computational overhead compared to existing approaches such as JTT [25] and CnC [49]. Unlike our method, JTT and CnC require retraining an additional

Table 3: Comparison of worst-group accuracy (WGA), average accuracy (Acc.), and accuracy gap across text datasets. Best worst-group accuracies are highlighted in boldface.  $^{\dagger}$  denotes using a fraction of validation data for model fine-tuning.

Method	Backbone	<b>Group Annotations</b>		MultiNLI			CivilComments		
Maria Succession	Duckbone	Train	Val	WGA(%)↑	Acc.(%) ↑	Gap(%) ↓	WGA(%)↑	Acc.(%) ↑	Gap(%) ↓
ERM [39]	BERT	-	-	67.9	82.4	14.5	57.4	92.6	35.2
JTT [25]	BERT	No	Yes	72.6	78.6	6.0	69.3	91.1	21.8
CNC [49]	BERT	No	Yes	-	-	-	$68.9_{\pm 2.1}$	$81.7_{\pm 0.5}$	12.8
BAM [24]	BERT	No	Yes	$71.2_{\pm 1.6}$	$79.6_{\pm 1.1}$	8.4	$79.3_{\pm 2.7}$	$88.3_{\pm 0.8}$	9.0
AFR [30]	BERT	No	Yes	$73.4_{\pm 0.6}$	$81.4_{\pm 0.2}$	8.0	$68.7_{\pm 0.6}$	$89.8_{\pm 0.6}$	21.1
$\mathrm{DFR}^{\dagger}$ [18]	BERT	No	Yes	$70.8_{\pm 0.8}$	$81.7_{\pm 0.2}$	10.9	$81.8_{\pm 1.6}$	$87.5_{\pm 0.2}$	5.7
SELF <sup>†</sup> [21]	BERT	No	Yes	$70.7_{\pm 2.5}$	$81.2_{\pm 0.7}$	10.5	$79.1_{\pm 2.1}$	$87.7_{\pm 0.6}$	8.6
LfF [28]	BERT	No	No	70.2	80.8	10.6	58.8	92.5	33.7
BAM [24]	BERT	No	No	$70.8_{\pm 1.5}$	$80.3_{\pm 1.0}$	9.5	$79.3_{\pm 2.7}$	$88.3_{\pm 0.8}$	9.0
Ours <sup>†</sup>	BERT	No	No	$\textbf{74.5}_{\pm 1.2}$	$80.6_{\pm0.8}$	7.3	$80.2_{\pm 0.9}$	$87.1_{\pm 0.4}$	6.9

Table 4: Worst-group (WGA) and average accuracy (Acc.) on the CheXpert dataset. All group robustness methods use the same half of the validation set. Best worst-group accuracies and average accuracies are highlighted in boldface.

Method	Backbone	WGA(%)↑	Acc.(%) ↑
ERM [39]	ResNet50	$22.0_{\pm 1.6}$	$90.8_{\pm 0.1}$
JTT [25]	ResNet50	60.4 <sub>±4.9</sub>	$75.2_{\pm0.8}$
DFR [18]	ResNet50	$72.7_{\pm 1.5}$	$78.7_{\pm 0.4}$
AFR [30]	ResNet50	$72.4_{\pm 2.0}$	$76.8_{\pm 1.1}$
Ours	ResNet50	$\textbf{73.6}_{\pm 1.1}$	$79.9_{\pm 0.9}$

model from scratch. In contrast, our method, which consists of a standard ERM training with evidence regularization and an evidential calibration, only manipulates the last-layer of the model. Thus, our approach is efficient in terms of both computation and memory.

### 5.5 Ablation Studies

In Figure 4, we present the effect of the annealing step  $\eta$  (from Equation (12)) and the regularization strength  $\beta$  (from Equation (15)), as well as how class balancing and our proposed KL (from Equation (12)) and weight (from Equation (15)) regularization contribute to group robustness.

Specifically, Figure 4(a) highlights the effectiveness of our proposed weight regularization when  $\beta > 0$ . Compared with no weight regularization when  $\beta = 0$ , our method benefits with a moderate  $\beta$ , e.g.,  $\beta = 10$  on the CelebA dataset. Figure 4(b) demonstrates the importance of KL regularization as well as how it is scheduled in the second-order risk minimization. We denote no such regularization with  $\eta = 0$ . When  $\eta = 20$ , which equals the total number of training epochs, the regularization strength is progressively increased until the end of training. When  $\eta < 20$ , the regularization strength peaks at the  $\eta$ 'th epoch and remains unchanged for the rest of training. In general, adding the KL regularization benefits finding good uncertainty estimations and thereby improves a model's group robustness. Selecting an appropriate  $\eta$  is dataset-dependent,

and in practice, a small  $\eta$  is favored for datasets with severe group imbalances, such as CelebA. Figure 4(c) analyzes how class balancing (CB) and our proposed regularizations (Reg) benefit from each other to achieve the optimal group robustness. Compared with NoCB-NoReg, which is the vanilla evidential calibration algorithm, adopting CB (denoted as CB-NoReg) improves group robustness to some extend. Our method, which incorporates both CB and Reg, provides better uncertainty estimations than NoCB-Reg and CB-NoReg and significantly boosts models' group robustness by achieving the highest worst-group accuracy.

Table 5: Comparison of other reweighting-based methods on computational complexity.

Method	Time Complexity
JTT	$O(NT  \xi_{\rm full})$
DFR	$O(N T_2 \xi_{\text{last}})$
AFR	$O(N T_2 \xi_{\text{last}} + N \xi_{fw})$
Ours	$O(N T_1 \xi_{\text{last}} + N T_2 \xi_{\text{last}})$

### 5.6 Complexity Analysis

We analyze the computational complexity of our method, Evidential Alignment, compared with other reweighting-based approaches such as JTT, DFR, and AFR (see Table 5). Let N denote the number of training samples. T is the number of epochs for full model training (used by JTT).  $T_1$  is the number of epochs for the second-order risk minimization stage in Evidential Alignment.  $T_2$  is the number of epochs for retraining only the last layer (used by DFR, AFR, and Evidential Alignment). We use  $\xi_{\text{full}}$  for the cost per sample per epoch in full model training and  $\xi_{\text{last}}$  for last-layer training, where  $\xi_{\text{full}} \gg \xi_{\text{last}}$ . For methods that train the full model over T epochs (i.e., JTT), the complexity is  $O(NT\xi_{\text{full}})$ . This induces the highest cost. In contrast, DFR retrains only the last layer for  $T_2$  epochs, yielding a complexity of  $O(NT\xi_{\text{last}})$ . Note that DFR requires group annotations. AFR extends DFR by precomputing

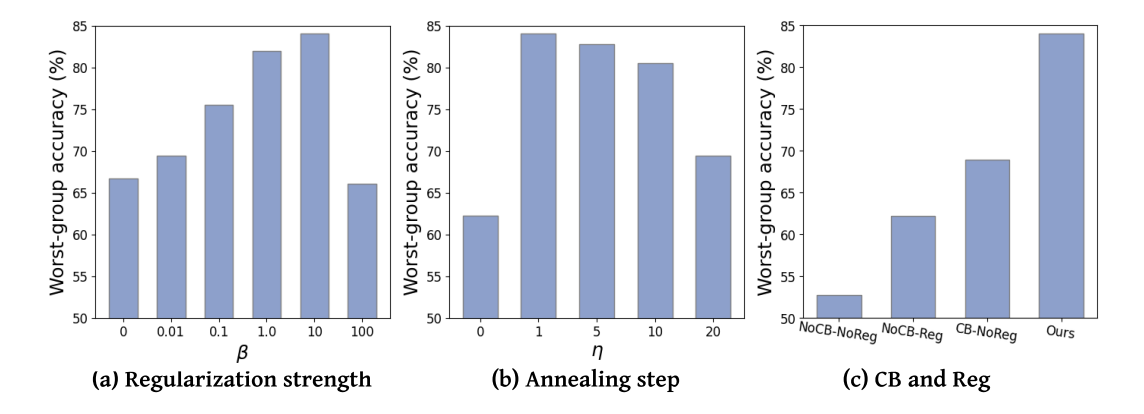


Figure 4: Ablation study on how (a) regularization strength  $\beta$ , (b) annealing step  $\eta$ , and (c) class balancing (CB) and regularization (Reg) affect our method's worst-group accuracy on the CelebA dataset.

sample losses. Let  $\xi_{fw}$  be the cost for a single feedforward operation per sample. AFR adds an extra cost of  $O(N\,\xi_{fw})$ . Evidential Alignment also efficiently uses last-layer training in both stages. First, the second-order risk minimization stage runs for  $T_1$  epochs. Then, last-layer retraining runs for  $T_2$  epochs. The overall complexity is  $O(N\,T_1\,\xi_{\rm last}+N\,T_2\,\xi_{\rm last})$ . Although Evidential Alignment has a slightly higher cost than DFR, it shares the same big-O notation as DFR and AFR, which offers a favorable trade-off between computational efficiency and improved group robustness.

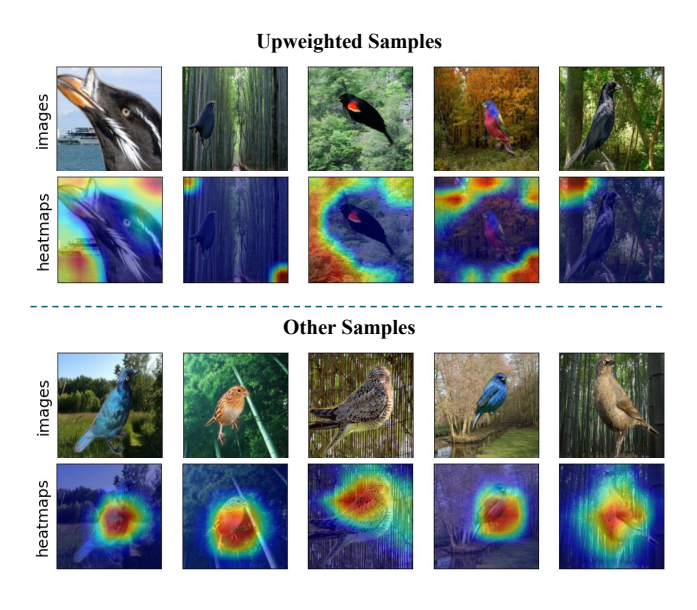


Figure 5: GradCAM [32] visualizations for the upweighted samples and other samples in the Waterbirds dataset.

# 5.7 Visualization of Reweighted Samples

A crucial aspect of Evidential Alignment is determining whether the model's epistemic uncertainty can effectively reflect the erroneous patterns in the biased ERM model. In our experiments on the Waterbirds dataset, we used GradCAM visualizations (Figure 5) to examine the areas of focus for samples with the highest and lowest uncertainty. We observed that high upweighted samples tended to focus background regions associated with the spurious attributes, while non-upweighted samples focused more on the birds themselves, showing our method's effectiveness on identifying potential spurious biases. Additionally, t-SNE embeddings (Figure 3) in our synthetic experiment also revealed that high-uncertainty samples clustered around minority groups in the feature space, further supporting the correlation between uncertainty and group information. Quantitative analysis showed correlations between uncertainty values and true group labels across all datasets, indicating that uncertainty estimates are reliable proxies for identifying underrepresented groups. These findings validate our approach of using uncertainty-aware reweighting during retraining, as it allows the model to prioritize learning from challenging and minority group samples, thereby enhancing overall group robustness.

### 6 Conclusion

In this work, we introduce a novel uncertainty-guided group robustness method, Evidential Alignment. Our framework demonstrates that leveraging existing observations from both the biased ERM model and the calibration dataset enables effective mitigation on spurious biases of the deep neural networks. Our method decompose the uncertainty and utilizes epistemic uncertainty from biased ERM models to inform the debiasing process. Extensive experiments demonstrate the efficacy of our approach, achieving favorable worst-group performance across diverse datasets in both vision and text. We believe this work provides valuable insights into developing more adaptive and scalable methods to improve group robustness in real-world applications.

### Acknowledgements

This work is supported in part by the US National Science Foundation under grants 2217071, 2213700, 2106913, 2008208. Any opinions, findings, and conclusions or recommendations expressed in this material are those of the author(s) and do not necessarily reflect the views of the National Science Foundation.

#### References

- Alexander Amini, Wilko Schwarting, Ava Soleimany, and Daniela Rus. 2020.
   Deep evidential regression. Advances in neural information processing systems 33 (2020), 14927–14937.
- [2] Martin Arjovsky, Léon Bottou, Ishaan Gulrajani, and David Lopez-Paz. 2019. Invariant risk minimization. arXiv preprint arXiv:1907.02893 (2019).
- [3] Nicholas Baker, Hongjing Lu, Gennady Erlikhman, and Philip J Kellman. 2018. Deep convolutional networks do not classify based on global object shape. PLoS computational biology 14, 12 (2018), e1006613.
- [4] Solon Barocas, Moritz Hardt, and Arvind Narayanan. 2023. Fairness and machine learning: Limitations and opportunities. MIT press.
- [5] Sara Beery, Grant Van Horn, and Pietro Perona. 2018. Recognition in terra incognita. In Proceedings of the European Conference on Computer Vision. 456– 473
- [6] David Bergman, André Augusto Ciré, Willem Jan van Hoeve, John N. Hooker, and Audun Jøsang. 2016. Subjective Logic: A Formalism for Reasoning Under Uncertainty. https://api.semanticscholar.org/CorpusID:86641091
- [7] Charles Blundell, Julien Cornebise, Koray Kavukcuoglu, and Daan Wierstra. 2015. Weight uncertainty in neural network. In *International conference on machine learning*. PMLR, 1613–1622.
- [8] Daniel Borkan, Lucas Dixon, Jeffrey Sorensen, Nithum Thain, and Lucy Vasserman. 2019. Nuanced metrics for measuring unintended bias with real data for text classification. In Companion proceedings of the 2019 world wide web conference. 491–500
- [9] Yarin Gal and Zoubin Ghahramani. 2016. Dropout as a bayesian approximation: Representing model uncertainty in deep learning. In international conference on machine learning. PMLR. 1050–1059.
- [10] Karan Goel, Albert Gu, Yixuan Li, and Christopher Ré. 2020. Model patching: Closing the subgroup performance gap with data augmentation. arXiv preprint arXiv:2008.06775 (2020).
- [11] Kaiming He, Xiangyu Zhang, Shaoqing Ren, and Jian Sun. 2016. Deep residual learning for image recognition. In Proceedings of the IEEE conference on computer vision and pattern recognition. 770–778.
- [12] Eyke Hüllermeier and Willem Waegeman. 2021. Aleatoric and epistemic uncertainty in machine learning: An introduction to concepts and methods. *Machine learning* 110, 3 (2021), 457–506.
- [13] Jeremy Irvin, Pranav Rajpurkar, Michael Ko, Yifan Yu, Silviana Ciurea-Ilcus, Chris Chute, Henrik Marklund, Behzad Haghgoo, Robyn Ball, Katie Shpanskaya, et al. 2019. Chexpert: A large chest radiograph dataset with uncertainty labels and expert comparison. In Proceedings of the AAAI conference on artificial intelligence, Vol. 33, 590–597.
- [14] Alex Kendall and Yarin Gal. 2017. What uncertainties do we need in bayesian deep learning for computer vision? Advances in neural information processing systems 30 (2017).
- [15] Jacob Devlin Ming-Wei Chang Kenton and Lee Kristina Toutanova. 2019. BERT: Pre-training of Deep Bidirectional Transformers for Language Understanding. In Proceedings of NAACL-HLT. 4171–4186.
- [16] Fereshte Khani and Percy Liang. 2021. Removing spurious features can hurt accuracy and affect groups disproportionately. In Proceedings of the 2021 ACM conference on fairness, accountability, and transparency. 196–205.
- [17] Nayeong Kim, Sehyun Hwang, Sungsoo Ahn, Jaesik Park, and Suha Kwak. 2022. Learning debiased classifier with biased committee. Advances in Neural Information Processing Systems 35 (2022), 18403–18415.
- [18] Polina Kirichenko, Pavel Izmailov, and Andrew Gordon Wilson. 2023. Last Layer Re-Training is Sufficient for Robustness to Spurious Correlations. In International Conference on Learning Representations.
- [19] Pang Wei Koh, Shiori Sagawa, Henrik Marklund, Sang Michael Xie, Marvin Zhang, Akshay Balsubramani, Weihua Hu, Michihiro Yasunaga, Richard Lanas Phillips, Irena Gao, et al. 2021. Wilds: A benchmark of in-the-wild distribution shifts. In *International Conference on Machine Learning*. PMLR, 5637–5664.
- [20] Tyler LaBonte, John C Hill, Xinchen Zhang, Vidya Muthukumar, and Abhishek Kumar. 2024. The Group Robustness is in the Details: Revisiting Finetuning under Spurious Correlations. arXiv preprint arXiv:2407.13957 (2024).
- [21] Tyler LaBonte, Vidya Muthukumar, and Abhishek Kumar. 2024. Towards lastlayer retraining for group robustness with fewer annotations. Advances in Neural Information Processing Systems 36 (2024).
- [22] Balaji Lakshminarayanan, Alexander Pritzel, and Charles Blundell. 2017. Simple and scalable predictive uncertainty estimation using deep ensembles. Advances in neural information processing systems 30 (2017).
- [23] Yann LeCun, Léon Bottou, Yoshua Bengio, and Patrick Haffner. 1998. Gradient-based learning applied to document recognition. Proc. IEEE 86, 11 (1998), 2278–2234.
- [24] Gaotang Li, Jiarui Liu, and Wei Hu. 2024. Bias Amplification Enhances Minority Group Performance. Transactions on Machine Learning Research (2024).
- [25] Evan Z Liu, Behzad Haghgoo, Annie S Chen, Aditi Raghunathan, Pang Wei Koh, Shiori Sagawa, Percy Liang, and Chelsea Finn. 2021. Just train twice: Improving group robustness without training group information. In *International Conference*

- $on\ Machine\ Learning.\ PMLR,\ 6781-6792.$
- [26] Ziwei Liu, Ping Luo, Xiaogang Wang, and Xiaoou Tang. 2015. Deep learning face attributes in the wild. In Proceedings of the IEEE International Conference on Computer Vision. 3730–3738.
- [27] Andrey Malinin and Mark Gales. 2018. Predictive uncertainty estimation via prior networks. Advances in neural information processing systems 31 (2018).
- [28] Junhyun Nam, Hyuntak Cha, Sungsoo Ahn, Jaeho Lee, and Jinwoo Shin. 2020. Learning from failure: De-biasing classifier from biased classifier. Advances in Neural Information Processing Systems 33 (2020), 20673–20684.
- [29] Junhyun Nam, Jaehyung Kim, Jaeho Lee, and Jinwoo Shin. 2022. Spread Spurious Attribute: Improving Worst-group Accuracy with Spurious Attribute Estimation. In International Conference on Learning Representations.
- [30] Shikai Qiu, Andres Potapczynski, Pavel Izmailov, and Andrew Gordon Wilson. 2023. Simple and fast group robustness by automatic feature reweighting. In International Conference on Machine Learning. PMLR, 28448–28467.
- [31] Shiori Sagawa, Pang Wei Koh, Tatsunori B Hashimoto, and Percy Liang. 2020. Distributionally Robust Neural Networks. In International Conference on Learning Representations
- [32] Ramprasaath R Selvaraju, Michael Cogswell, Abhishek Das, Ramakrishna Vedantam, Devi Parikh, and Dhruv Batra. 2020. Grad-CAM: visual explanations from deep networks via gradient-based localization. *International journal of computer vision* 128 (2020), 336–359.
- [33] Murat Sensoy, Lance Kaplan, and Melih Kandemir. 2018. Evidential deep learning to quantify classification uncertainty. Advances in neural information processing systems 31 (2018).
- [34] Seonguk Seo, Joon-Young Lee, and Bohyung Han. 2022. Unsupervised learning of debiased representations with pseudo-attributes. In Proceedings of the IEEE/CVF Conference on Computer Vision and Pattern Recognition. 16742–16751.
- [35] Nimit Sohoni, Jared Dunnmon, Geoffrey Angus, Albert Gu, and Christopher Ré. 2020. No subclass left behind: Fine-grained robustness in coarse-grained classification problems. Advances in Neural Information Processing Systems 33 (2020), 19339–19352.
- [36] Pierre Stock and Moustapha Cisse. 2018. Convnets and imagenet beyond accuracy: Understanding mistakes and uncovering biases. In Proceedings of the European Conference on Computer Vision (ECCV). 498–512.
- [37] Dennis Ulmer, Christian Hardmeier, and Jes Frellsen. 2021. Prior and posterior networks: A survey on evidential deep learning methods for uncertainty estimation. arXiv preprint arXiv:2110.03051 (2021).
- [38] Laurens Van der Maaten and Geoffrey Hinton. 2008. Visualizing data using t-SNE. Journal of machine learning research 9, 11 (2008).
- [39] Vladimir N Vapnik. 1999. An overview of statistical learning theory. IEEE transactions on neural networks (1999).
- [40] Jiaheng Wei, Harikrishna Narasimhan, Ehsan Amid, Wen-Sheng Chu, Yang Liu, and Abhishek Kumar. 2023. Distributionally robust post-hoc classifiers under prior shifts. arXiv preprint arXiv:2309.08825 (2023).
- [41] P. Welinder, S. Branson, T. Mita, C. Wah, F. Schroff, S. Belongie, and P. Perona. 2010. Caltech-UCSD Birds 200. Technical Report CNS-TR-2010-001. California Institute of Technology.
- [42] Adina Williams, Nikita Nangia, and Samuel R Bowman. 2017. A broad-coverage challenge corpus for sentence understanding through inference. arXiv preprint arXiv:1704.05426 (2017).
- [43] Ronald R. Yager and Liping Liu. 2010. Classic Works of the Dempster-Shafer Theory of Belief Functions. In Classic Works of the Dempster-Shafer Theory of Belief Functions. https://api.semanticscholar.org/CorpusID:54105362
- [44] Yuzhe Yang, Haoran Zhang, Dina Katabi, and Marzyeh Ghassemi. 2023. Change is hard: a closer look at subpopulation shift. In Proceedings of the 40th International Conference on Machine Learning. 39584–39622.
- [45] Huaxiu Yao, Yu Wang, Sai Li, Linjun Zhang, Weixin Liang, James Zou, and Chelsea Finn. 2022. Improving out-of-distribution robustness via selective augmentation. In *International Conference on Machine Learning*. PMLR, 25407–25437.
- [46] Wenqian Ye, Guangtao Zheng, Xu Cao, Yunsheng Ma, and Aidong Zhang. 2024. Spurious Correlations in Machine Learning: A Survey. http://arxiv.org/abs/2402. 12715 arXiv:2402.12715 [cs].
- [47] John R Zech, Marcus A Badgeley, Manway Liu, Anthony B Costa, Joseph J Titano, and Eric Karl Oermann. 2018. Variable generalization performance of a deep learning model to detect pneumonia in chest radiographs: a cross-sectional study. PLoS medicine 15, 11 (2018), e1002683.
- [48] Jianyu Zhang, David Lopez-Paz, and Léon Bottou. 2022. Rich feature construction for the optimization-generalization dilemma. In *International Conference on Machine Learning*. PMLR, 26397–26411.
- [49] Michael Zhang, Nimit S. Sohoni, Hongyang R. Zhang, Chelsea Finn, and Christopher Re. 2022. Correct-N-Contrast: a Contrastive Approach for Improving Robustness to Spurious Correlations. In Proceedings of the 39th International Conference on Machine Learning. PMLR, 26484–26516. https://proceedings.mlr.press/v162/ zhang22z.html ISSN: 2640-3498.
- [50] Guangtao Zheng, Wenqian Ye, and Aidong Zhang. 2024. Benchmarking Spurious Bias in Few-Shot Image Classifiers. In European Conference on Computer Vision. Springer, 346–364.

- [51] Guangtao Zheng, Wenqian Ye, and Aidong Zhang. 2024. Learning Robust Classifiers with Self-Guided Spurious Correlation Mitigation. http://arxiv.org/abs/2405.03649 arXiv:2405.03649 [cs].
- [52] Guangtao Zheng, Wenqian Ye, and Aidong Zhang. 2024. Spuriousness-Aware Meta-Learning for Learning Robust Classifiers. http://arxiv.org/abs/2406.10742 arXiv:2406.10742 [cs].
- [53] Guangtao Zheng, Wenqian Ye, and Aidong Zhang. 2025. ShortcutProbe: Probing Prediction Shortcuts for Learning Robust Models. arXiv preprint arXiv:2505.13910 (2025).
- [54] Bolei Zhou, Agata Lapedriza, Aditya Khosla, Aude Oliva, and Antonio Torralba. 2017. Places: A 10 million image database for scene recognition. *IEEE Transactions on Pattern Analysis and Machine Intelligence* 40, 6 (2017), 1452–1464.

# **Appendix**

# A Dataset Distributions

By examining the distributions of the four datasets, we can observe distinct patterns of group/class imbalance shown in Table 6. For the Waterbirds and MultiNLI datasets, although group imbalances are present, the overall class distribution is nearly balanced. In contrast, both group and class imbalances are observed in the CelebA and CivilComments datasets. The CheXpert dataset differs by including more spurious attributes (combination of race (White, Black, Other) and gender (Male, Female)), reflecting a more complex real-world scenario. This variation suggests that applying simple techniques, such as class-balancing or group-balancing, may have different impacts on improving group robustness, depending on the specific characteristics of the dataset. Recent work by LaBonte et al. [20] also emphasizes that existing class-balancing strategies can produce inconsistent results across these datasets. This underscores the need for a deeper understanding of group robustness, particularly in realworld applications. Consequently, it is crucial to develop adaptive methods that can more effectively address both class and group imbalances to enhance group robustness across diverse datasets.

### **B** More Experimental Results

**Hyperparameter Selection.** We include the hyperparameter selection for both second-order risk minimization and evidential calibration in Table 9 and Table 10, respectively. We select hyperparameters based on the convergence in training and the performance on the validation data. For example, a too small or too large learning rate hinders the convergence of our algorithm. The annealing step  $\eta$  and regularization strength  $\beta$  are chosen similarly. The overall performance is robust to small variations in these values.

**Backbone Models.** In the main paper, we choose ResNet-50 and BERT (base) as the backbones for experiments, as they were commonly used in previous works. To further validate the effectiveness, we added more experiments with ViT-base pretrained on both ImageNet 1K and ImageNet 21K, shown in Table 7. The results show that our method is also effective in improving group robustness in a backbone agnostic manner.

**Sensitivity analysis.** To ensure a fair comparison with other baselines, we used half of the validation set as the calibration set in the paper. However, our method is flexible and can work with different calibration set sizes. Table 8 presents experiments with various portions of the validation set as calibration sets on the Waterbirds dataset. The results indicate that a larger and more diverse calibration set further improves group robustness against spurious correlations.

Table 6: Data quantities and group compositions for each dataset, including training, validation, and test splits.

Dataset	Classii	C	Train	Validation	Test
Dataset	Class y	Spurious a	1 rain	validation	rest
		Waterbirds			
Waterbirds	landbird	land	3498	467	2225
Waterbirds	landbird	water	184	466	2225
Waterbirds	waterbird	land	56	133	642
Waterbirds	waterbird	water	1057	133	642
		CelebA			
CelebA	non-blond	female	71629	8535	9767
CelebA	non-blond	male	66874	8276	7535
CelebA	blond	female	22880	2874	2480
CelebA	blond	male	1387	182	180
		MultiNLI			
MultiNLI	contradiction	no negation	57498	22814	34597
MultiNLI	contradiction	negation	11158	4634	6655
MultiNLI	entailment	no negation	67376	26949	40496
MultiNLI	entailment	negation	1521	613	886
MultiNLI	neither	no negation	66630	26655	39930
MultiNLI	neither	negation	1992	797	1148
		CivilComments			
CivilComments	neutral	no identity	148186	25159	74780
CivilComments	neutral	identity	90337	14966	43778
CivilComments	toxic	no identity	12731	2111	6455
CivilComments	toxic	identity	17784	2944	8769
		CheXpert			
CheXpert	finding	(race, gender)	129434	185	614
CheXpert	no-finding	(race, gender)	61593	49	54

Table 7: Experiments on Waterbirds with more backbones.

Backbone	Pretraining	Method	WGA
ResNet-50	ImageNet 1K	ERM	72.6
ResNet-50	ImageNet 1K	Ours	92.2
ViT-base	ImageNet 1K	ERM	49.4
ViT-base	ImageNet 1K	Ours	86.4
ViT-base	ImageNet 21K	ERM	69.9
ViT-base	ImageNet 21K	Ours	86.8

Table 8: Sensitivity Analysis on the size of calibration sets. Portion denotes the portion of the validation set used for calibration sets.

Portion	Acc.	WGA	Gap
0.1	95.7	83.0	12.7
0.2	95.0	89.7	5.3
0.3	96.3	91.1	5.2
0.4	96.2	91.9	4.3
0.5	95.1	92.2	2.9

# **C** Proofs of Theoretical Analysis

# C.1 Proof of Theorem 4.1

PROOF. We start from the KL divergence between the variational approximation  $p(\pi|x, \theta)$  and the true posterior  $p(\pi|y)$ :

$$KL\left[p(\boldsymbol{\pi}|\boldsymbol{x},\boldsymbol{\theta}) \parallel p(\boldsymbol{\pi}|\boldsymbol{y})\right] = \mathbb{E}_{p(\boldsymbol{\pi}|\boldsymbol{x},\boldsymbol{\theta})} \left[\log \frac{p(\boldsymbol{\pi}|\boldsymbol{x},\boldsymbol{\theta})}{p(\boldsymbol{\pi}|\boldsymbol{y})}\right]. \tag{20}$$

Hyperparameters	Waterbirds	CelebA	MultiNLI	CivilComments	CheXpert
initial learning rate	3e-3	3e-3	1e-3	1e-3	1e-3
epochs	50	100	100	100	100
annealing step $(\eta)$	10	1	1	1	1
learning rate scheduler	CosineAnnealing	CosineAnnealing	Linear	Linear	Linear
optimizer	SGD	SGD	AdamW	AdamW	SGD
weight decay	1e-4	1e-4	1e-4	1e-4	1e-4
batch size	32	128	128	128	128
backbone	ResNet-50	ResNet-50	BERT	BERT	ResNet-50

Table 9: Hyperparameters for second-order risk minimization.

Table 10: Hyperparameters for evidential calibration.

Hyperparameters	Waterbirds	CelebA	MultiNLI	CivilComments	CheXpert
learning rate	1e-3	2e-2	1e-5	1e-3	1e-2
epochs	100	200	200	200	200
regularization strength $(\beta)$	10	10	10	10	10
optimizer	SGD	SGD	SGD	SGD	SGD
batch size	128	128	128	128	128
backbone	ResNet-50	ResNet-50	BERT	BERT	ResNet-50

Using Bayes' rule, we get

$$p(\boldsymbol{\pi}|\boldsymbol{y}) = \frac{p(\boldsymbol{y}|\boldsymbol{\pi})p(\boldsymbol{\pi})}{p(\boldsymbol{y})},\tag{21}$$

we rewrite the KL divergence as:

$$\mathrm{KL}[p(\boldsymbol{\pi}|\boldsymbol{x},\boldsymbol{\theta}) \parallel p(\boldsymbol{\pi}|\boldsymbol{y})] = \mathbb{E}_{p(\boldsymbol{\pi}|\boldsymbol{x},\boldsymbol{\theta})} \left[ \log \frac{p(\boldsymbol{\pi}|\boldsymbol{x},\boldsymbol{\theta})}{P(\boldsymbol{y}|\boldsymbol{\pi})p(\boldsymbol{\pi})} \right] + \log p(\boldsymbol{y}). \tag{22}$$

Since KL divergence is non-negative, we obtain the evidence lower bound (ELBO):

$$\log p(y) \ge \mathbb{E}_{p(\boldsymbol{\pi}|\boldsymbol{x},\boldsymbol{\theta})}[\log P(y|\boldsymbol{\pi})] - \mathrm{KL}[p(\boldsymbol{\pi}|\boldsymbol{x},\boldsymbol{\theta}) \parallel p(\boldsymbol{\pi})]. \quad (23)$$

Rearranging, we obtain the ELBO:

$$\mathcal{L}_{\text{ELBO}} = -\mathbb{E}_{p(\boldsymbol{\pi}|\boldsymbol{x},\boldsymbol{\theta})}[\log P(\boldsymbol{y}|\boldsymbol{\pi})] + \text{KL}[p(\boldsymbol{\pi}|\boldsymbol{x},\boldsymbol{\theta}) \parallel p(\boldsymbol{\pi})]. \quad (24)$$

By parameterizing  $p(\pi|\mathbf{x},\theta)$  as a Dirichlet distribution with parameters  $\alpha$ , we use known properties of the KL divergence between Dirichlet distributions and obtain:

$$\mathcal{L}_{\text{ELBO}} = \psi(\alpha_y) - \psi(\alpha_0) - \log \frac{B(\boldsymbol{\alpha})}{B(\boldsymbol{\gamma})} + \sum_{k=1}^{K} (\alpha_k - \gamma_k)(\psi(\alpha_k) - \psi(\alpha_0)),$$
(25)

which is the evidence regularization term controlling confidence in predictions and  $\psi(z) = \frac{d}{dz} \ln \Gamma(z)$  is the digamma function. Therefore, minimizing the second-order risk optimizes the ELBO, leading to a model that learns evidence from predictions.

#### C.2 Proof of Theorem 4.2

PROOF. Fix any group  $g \in \{1, ..., |\mathcal{G}|\}$ . Since we have  $n_g$  i.i.d. training samples from group g, a standard PAC-Bayes argument for [0,1]-bounded loss implies that for any  $0 < \delta_q < 1$ , with probability

at least  $1 - \delta_g$  over the sample of group g,

$$\mathbb{E}_{f \sim Q}[R_g(f)] \leq \mathbb{E}_{f \sim Q}[\hat{R}_g(f)] + \sqrt{\frac{\mathrm{KL}(Q||P) + \ln(\frac{1}{\delta_g})}{2 \, n_g}}. \tag{26}$$

By choosing  $\delta_g = \delta/|\mathcal{G}|$  and applying a union bound, we have that, with probability at least  $1 - \delta$ , every group satisfies

$$\mathbb{E}_{f \sim Q}[R_g(f)] \le \mathbb{E}_{f \sim Q}[\hat{R}_g(f)] + \sqrt{\frac{\text{KL}(Q||P) + \ln(\frac{|\mathcal{G}|}{\delta})}{2 n_q}}$$
(27)

simultaneously. Taking the maximum over g and noting that  $n_g \ge n_{\min}$ , we obtain

$$\max_{1 \le g \le |\mathcal{G}|} \mathbb{E}_{f \sim Q}[R_g(f)] \tag{28}$$

$$\leq \max_{g} \left\{ \mathbb{E}_{f \sim Q} \left[ \hat{R}_{g}(f) \right] + \sqrt{\frac{\mathrm{KL}(Q \| P) + \ln\left(\frac{|\mathcal{G}|}{\delta}\right)}{2 \, n_{g}}} \right\} \tag{29}$$

$$\leq \max_{g} \mathbb{E}_{f \sim Q} [\hat{R}_{g}(f)] + \sqrt{\frac{\mathrm{KL}(Q \| P) + \ln(\frac{|\mathcal{G}|}{\delta})}{2 \, n_{\min}}}. \tag{30}$$

Since  $\hat{R}_w(f)$  is a convex combination of the group-wise empirical risks, let  $a_g = \mathbb{E}_{f \sim Q}[\hat{R}_g(f)]$ . We then have

$$\max_g \, a_g \leq \frac{1}{\min_{g'} w_{g'}} \sum_{g=1}^{|\mathcal{G}|} w_g a_g = \frac{1}{\alpha} \mathbb{E}_{f \sim Q} \big[ \hat{R}_w(f) \big].$$

Combining these bounds completes the proof:

$$\max_{1 \leq g \leq |\mathcal{G}|} \mathbb{E}_{f \sim Q}[R_g(f)] \leq \frac{1}{\alpha} \mathbb{E}_{f \sim Q}[\hat{R}_w(f)] + \sqrt{\frac{\mathrm{KL}(Q \| P) + \ln\left(\frac{|\mathcal{G}|}{\delta}\right)}{2 \, n_{\min}}}.$$